Lab on a Chip

PAPER

View Article Online
View Journal

Cite this: DOI: 10.1039/c5lc01413a

Effects of molecular confinement and crowding on horseradish peroxidase kinetics using a nanofluidic gradient mixer†

William R. A. Wichert,[a] Donghoon Han[b] and Paul W. Bohn*[ab]

Received 17th November 2015,
Accepted 8th January 2016

DOI: 10.1039/c5lc01413a

www.rsc.org/loc

The effects of molecular confinement and crowding on enzyme kinetics were studied at length scales and under conditions similar to those found in biological cells. These experiments were carried out using a nanofluidic network of channels constituting a nanofluidic gradient mixer, providing the basis for measuring multiple experimental conditions simultaneously. The 100 nm × 40 μm nanochannels were wet etched directly into borosilicate glass, then annealed and characterized with fluorescein emission prior to kinetic measurements. The nanofluidic gradient mixer was then used to measure the kinetics of the conversion of the horseradish peroxidase (HRP)-catalyzed conversion of non-fluorescent Amplex Red (AR) to the fluorescent product resorufin in the presence of hydrogen peroxide (H_2O_2). The design of the gradient mixer allows reaction kinetics to be studied under multiple (five) unique solution compositions in a single experiment. To characterize the efficiency of the device the effects of confinement on HRP-catalyzed AR conversion kinetics were studied by varying the starting ratio of AR : H_2O_2. Equimolar concentrations of Amplex Red and H_2O_2 yielded the highest reaction rates followed by 2 : 1, 1 : 2, 5 : 1, and finally 1 : 5 [AR] : [H_2O_2]. Under all conditions, initial reaction velocities were decreased by excess H_2O_2. Crowding effects on kinetics were studied by increasing solution viscosity in the nanochannels in the range 1.0–1.6 cP with sucrose. Increasing the solution viscosities in these confined geometries decreases the initial reaction velocity at the highest concentration from 3.79 μM min^{-1} at 1.00 cP to 0.192 μM min^{-1} at 1.59 cP. Variations in reaction velocity are interpreted in the context of models for HRP catalysis and for molecular crowding.

Introduction

Lab-on-a-chip devices have been fabricated with increasing complexity as the characteristic dimensions are reduced from the millimeter to the micrometer scale. Devices, typically made from glass,[1] polystyrene,[2] PDMS,[3] and now 3D printing,[4] have been used for a wide variety of biological applications including *in vitro* cellular analysis,[5,6] biological communication,[7] and enzyme kinetics.[8–10] With the increasing availability of nanofabrication capabilities, lab-on-a-chip devices have begun to exploit nanoscale properties[11–13] in the physical form of nanopores,[14–16] glass fiber bundles,[17] and nanochannels.[18] Nanoscale devices have been fabricated in a number of ways including wet-chemical etching, nanosphere lithography, focused ion beam (FIB) milling, and electron beam lithography.[19–23] Nanopores are usually fabricated by nanosphere lithography or FIB, while nanochannels are typically made by FIB milling which permits control over channel dimensions simply by altering the ion-beam current.[24,25]

Utilization of nanopores in track-etched membranes has proven to be an especially useful addition to fluidic devices,[26–28] aiding in gas separations, protein analysis and nanofiltration through application of polymer brushes.[29,30] Bruening *et al.*, for example, immobilized poly(styrene sulfonate) and trypsin inside of membrane pores to increase the speed and efficiency of protein digestion.[31] One key issue affecting reaction kinetics of immobilized enzymes and other proteins in nanoscale architectures is the protein configuration and the potential for steric hindrance that needs to be considered when utilizing surface-immobilized biomacromolecules. Alternatively, if reagent use issues are not limiting, then using non-immobilized enzymes can yield higher efficiency reactors and produce results that are more readily connected to *in vivo* kinetics.[32,33]

Nanoscale devices are of particular interest for studying how molecular confinement affects reaction efficiency at cellular and molecular length scales.[17,27,34,35] In previous work

[a] Department of Chemistry and Biochemistry, University of Notre Dame, Notre Dame, IN 46556, USA. E-mail: pbohn@nd.edu
[b] Department of Chemical and Biomolecular Engineering, University of Notre Dame, Notre Dame, IN 46556, USA

† Electronic supplementary information (ESI) available. See DOI: 10.1039/c5lc01413a

from our laboratory, the kinetics of horseradish peroxidase (HRP) immobilized in a track-etched membrane were studied by measuring the production of a fluorescent product (resorufin) from non-fluorescent reagents (Amplex Red and H_2O_2) downstream of the membrane in a polydimethylsiloxane (PDMS) microchannel.[27] Unfortunately, because the nanopores were oriented perpendicular to the membrane surface, it was not possible to follow the progress of the reaction spatially, a difficulty when trying to measure kinetics in real-time. Utilizing nanofluidic channels that are aligned parallel to the substrate surface is a useful alternative to perpendicularly-oriented nanopores, because the entire length of the nanochannel is accessible to optical interrogation, and the reaction extent can be measured directly as a function of position, and reaction velocities can be obtained directly by imaging.

Horseradish peroxidase (HRP) is an excellent model enzyme, as it can accept a range of substrates, but it possesses only a single well-characterized catalytic site, a heme prosthetic group.[36] It has been immobilized to solid substrates in a variety of configurations, retaining its activity even in the presence of possible complications due to steric hindrance.[37] HRP is known to oxidize both Scopoletin[38] as well as Amplex Red (AR),[39] making it possible to measure its enzymatic activity by monitoring product fluorescence, since the overall reaction is fluorogenic. The AR reaction is favored over Scopoletin due to its favorable extinction coefficient and the quantum efficiency of the product resorufin, as well as the fact that it exhibits an increase in fluorescence upon oxidation, rather than a decrease, as with Scopoletin. In addition, the mechanism of oxidation of AR is now well-understood, involving an initial one electron transfer from H_2O_2 to form an Fe(IV) oxo intermediate, which is followed by a pair of 1-electron/1-proton transfers and a final step in which two Amplex Red radicals undergo a dismutation reaction to form one molecule each of resorufin and Amplex Red.[17] Finally, HRP is a 44 kDa protein with an approximate molecular size of 6.0 nm × 3.5 nm × 3.0 nm, so it occupies a significant fraction of the height (≤100 nm) of the nanochannels developed for this work, making it a good candidate to study the effects of molecular confinement.[40]

In order to accurately mimic the behavior of the enzyme *in vivo*, measurements of enzyme kinetics should ideally reproduce the conditions found in the cell. The difficulty in doing so is that the composition of the cellular cytosol is highly variable with varying effects on both molecular transport[41,42] and reactivity,[43] although current understanding suggests that molecular crowding increases rates for reactions, like slow association reactions, that are limited by intrinsic chemical characteristics of the activation barrier, while it decreases rates for diffusion-limited reactions. This is consistent with the observation that diffusion is slowed in the cytosol by a few-fold in relation to diffusion in aqueous solutions of the same viscosity but without macromolecular crowding.[43]

In order to efficiently probe multiple reaction conditions in the shortest possible time, fluidic mixing may be utilized in order to obtain multiple sets of experimental conditions within a single experimental run. Integrating a fluidic gradient mixer on-chip has been shown to be an efficient way to generate spatial and temporal gradients of analyte concentration for use in downstream experiments.[44] Thus, as a first step towards developing a robust and broadly applicable experimental system capable of probing biomacromolecular reactions over wide ranges of conditions simulating the cytosol, we have developed a nanofluidic gradient mixer capable of simultaneously producing multiple homogeneous solution reaction conditions at different locations on the chip. Expanding on a wet-etching method used for microchannels,[19] we developed a technique for controllably etching channels in borosilicate glass to produce channel depths ranging from 40–100 nm, thus realizing nanofluidic geometries with aspect (width-to-depth) ratios exceeding 500. This architecture thus supports an electrokinetically-driven nanofluidic gradient mixer that takes two arbitrary initial concentrations of reactants and mixes them through a series of bifurcated and trifurcated channels, yielding a lateral (relative to the direction of flow) spatial concentration gradient ranging between the two starting concentrations. This gradient is then introduced, *via* electrokinetic flow, into a series of five reaction channels, arranged parallel to the glass surface (*i.e.* horizontal nanochannels). Once the reactants have been introduced into the reaction channels, the electrokinetic flow is stopped and the progress of the reaction is followed by fluorescence microscopic imaging. This device architecture allows multiple concentrations and conditions to be tested simultaneously. The nanofluidic mixer was characterized by measuring the effects of confinement and crowding on the kinetics of the HRP-catalyzed conversion of Amplex Red to resorufin.

Experimental

Materials

Schott Glass D substrates were purchased from Applied Microarrays; S1813 photoresist from Fisher Scientific; horseradish peroxidase, hydrogen peroxide, and sucrose from Sigma-Aldrich; and Amplex Red from Life Technologies. All solutions were prepared using 50 mM phosphate buffer (pH 7.4) and deionized (DI) water ($\rho \sim 18.2$ MΩ cm, EMD Millipore). A 10 mM stock solution of AR was prepared by dissolving in DMSO (Fisher Scientific).

Nanochannel fabrication

Nanofluidic devices were fabricated using conventional photolithography and wet chemical etching. Widths were controlled precisely using a chrome photomask while depths were controlled by varying the etch periods. Following a 60 s vapor deposition of hexamethyldisilazane (HMDS), the gradient mixer design was transferred to a photoresist covered glass substrate *via* a 5 s UV exposure at 14 mW cm^{-2} (Karl Suss MJB 3 mask aligner). After the development of photoresist in AZ917-MIF developer, the nanochannels were etched

with a 2 : 1 : 1 v : v : v mixture of 15 mM HF, 7.5 mM NH_4F, 7.5 mM HNO_3 etch solution to a typical depth of 100 nm and width of 40 μm. Channel dimensions were characterized using a stylus-based profilometer (Tencor P-6, KLA-Tencor Instruments) (ESI† Fig. S1). Fluidic access holes were drilled at the ends of the channels as a means to introduce solutions and permit electrode placement to drive electrokinetic flow.

Device annealing

Blank glass substrates and glass substrates containing the etched nanochannels were first subjected to high pressure DI water and then sonicated to remove residual glass particles from drilling the fluidic access holes. These substrates were then placed in a 3 : 1 piranha ($H_2SO_4 : H_2O_2$) solution for 30 min, rinsed with DI water, and immersed in 3 : 1 : 1 RCA solution ($NH_4OH : H_2O_2 : H_2O$) at 60 °C for 30 min. Finally the glass substrates were rinsed with DI water and annealed at 560 °C for 8 h. Prior to use, devices were filled with buffer and left overnight to ensure a uniform surface charge density.

Enzyme kinetics measurements

The positions of reactants and enzyme (AR, H_2O_2, HRP) were controlled electrokinetically with a high voltage sequencer (HVS448, LabSmith, Inc.) using the voltage scheme in Fig. 1. Electrokinetic flow was used to introduce the reactants through the mixer portion of the device and into the reaction channels for a period of 5 min, after which, the external voltage was shut off, and fluorescence measurements were acquired 1 min^{-1} for the remainder of the experiment using an inverted optical microscope (IX-71, Olympus, Inc.). Care was taken to shutter the excitation source between data acquisitions to avoid photooxidation of AR. A mercury arc lamp was used as the excitation source with appropriate excitation, dichroic and emission filters (AT540/25x, AT565DC, AT605/55m, Chroma). Initial rates were then calculated by first converting resorufin fluorescence intensity into concentration using a calibration curve (see ESI† Fig. S2) then calculating the initial slope of the kinetic curves (ESI† Fig. S3). Initial starting ratios of 1 : 1, 1 : 2, 1 : 5, 2 : 1, and 5 : 1 100 μM AR : 100 μM H_2O_2 with 0.025 units per mL (2.3 nM) HRP were examined. In these experiments, n : 1 represents a solution in which n = 100 μM and the other reactant concentration is $(1/n) \times 100$ μM.

Crowding measurements

Molecular crowding experiments were conducted using sucrose as the viscogen over a range of concentrations/viscosities. AR (100 μM), HRP (2.3 nM), and hydrogen peroxide (100 μM) solutions were prepared using 0, 5, 10, and 15% sucrose solutions, yielding viscosities ranging from 1.0–1.6 cP. Analytes were introduced and studied in the same manner as with the concentration and confinement measurements. Initial rates were again used to compare kinetic effects under crowding conditions.

Results and discussion

Device design and fabrication

Microfluidic gradient mixers have been built and demonstrated to generate spatial and temporal gradients of concentration with a great deal of flexibility in controlling design parameters with fabrication choices.[44] The design explored here is an electrokinetically-driven nanofluidic gradient mixer that takes two initial reactant concentrations and mixes them through a series of intersecting channels, yielding a lateral (relative to the direction of flow) spatial concentration gradient ranging between the two starting concentrations. This gradient is then introduced into a series of reaction channels, allowing multiple concentrations to be tested simultaneously. In the design tested here, five separate reactions channels

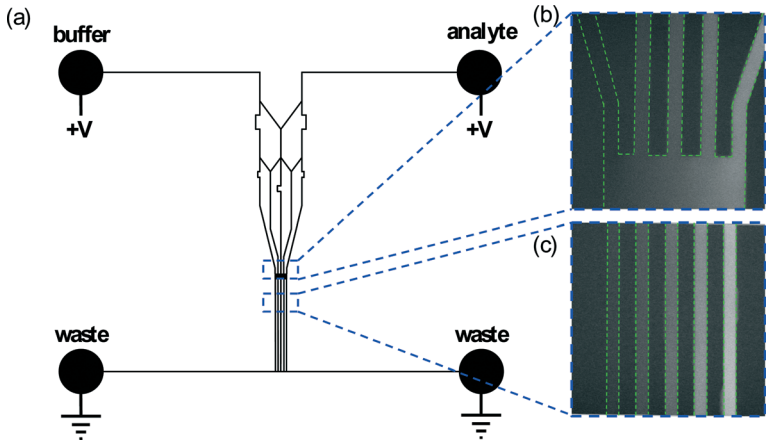

Fig. 1 Schematic diagram of the electrokinetically driven nanofluidic gradient mixer, permitting multiple concentration experiments to be carried out simultaneously. (a) Buffer is introduced along with reactant and mixed through a series of intersecting channels to form a concentration gradient in the lateral direction. (b) Fluorescence image of the device filled with 100 μM fluorescein and buffer acquired from the gradient column just above the lateral diffusion region. (c) Fluorescence image of the device acquired with 100 μM fluorescein and buffer obtained in the reaction nanochannels, illustrating that each nanochannel contains a unique, laterally-varying concentration of reactant.

were built, although the number can be increased as desired to characterize the reaction of interest. The nanofluidic mixer was initially characterized by imaging the mixing of 100 μM fluorescein with 50 mM pH 7.4 phosphate buffer, as shown in Fig. 1. As a model enzymatic reaction the effects of confinement and crowding on the kinetics of the HRP-catalyzed fluorogenic conversion of AR to resorufin in the presence of an oxidant (H_2O_2 here), Scheme 1, were studied. The formation of the highly fluorescent product, resorufin, was monitored by imaging the fluorescence from multiple nanochannels, each exhibiting a different composition, the resulting integrated fluorescence intensities then being used to determine reaction kinetics at multiple reaction conditions simultaneously in the nanofluidic gradient mixer.

Rectangular nanochannels were fabricated in glass using standard photolithography and wet chemical etching to produce the gradient mixer depicted in Fig. 1. The resulting device consists of a series of intersecting channels that permit mixing of analytes and flow into the gradient column which combines the contents of the mixing channels, yielding a concentration gradient ranging between each of the starting reactant concentrations. The gradient column provides each reaction channel with a unique concentration of analytes, allowing reactions to be carried out under multiple conditions and studied simultaneously. In a typical device the etched nanochannels were measured by profilometry to be 93 ± 12 nm in depth and 40 μm in width, as shown graphically in ESI† Fig. S1.

To assess the flow dynamics and mixing behavior, finite element simulations were performed over a two-dimensional domain representing the geometry and dimensions of the mixer employed in these experiments. A laminar flow, electrostatics, stationary study using transport of dilute species was carried out in order to simulate how samples mix with the sheath solution. Within the mixer, the flow velocity, u, is dictated by the incompressible Navier–Stokes equation,

$$\rho(u\cdot\nabla)u = \nabla\cdot[-pI + \mu(\nabla u + (\nabla u)^T)] + F \quad (1)$$

where ρ is the fluid density, p is the pressure, I is the identity metric, μ is the dynamic viscosity, and F is a volume force, such as gravity. The local concentration of the reactant is the main result followed in the simulations and is governed by Fick's law, which is described by the diffusion and convection equation:

$$\nabla\cdot(-D\nabla c) + u\cdot\nabla c = R$$

where D is the diffusion coefficient of the reactant, c is the concentration of the reactant, and R is the consumption rate of the reactant. Fig. 2 illustrates the simulated concentration profile as a function of position throughout the mixer. As shown, the simulations of gradient mixer produce a linear concentration range across the five reaction channels, consistent with fluorescence measurements shown in Fig. 1.

Nanofluidic channel measurements

It is by now well-appreciated that nanofluidic flow differs substantially from flow in larger, even microfluidic, channels,[45] so the initial studies examined the use of the nanofluidic gradient mixer to characterize the HRP-catalyzed conversion of AR to resorufin in the presence of H_2O_2, utilizing the nanofluidic gradient mixer and fluorescence microscopy. To introduce AR, H_2O_2, and HRP, 100 V is applied across the device (top to bottom). The resulting fluid flow mixes reactants and buffer, forming a concentration gradient at the gradient column that introduces unique concentrations into each of the reaction channels. Fig. S3† shows the fluorescence response with time in a typical experiment. Raw fluorescence data were acquired at a rate 1 min^{-1} over a period of 1 h and were converted to resorufin concentration using a standard working curve (Fig. S2†). The initial slope of the fluorescence response was used to determine the initial reaction rates, the determination of which provides a means of characterizing the effect of starting reactant concentration ratio and insight into how the nanofluidic geometry affects reaction velocity. The results are depicted in Fig. 3, where the initial reaction velocities, r_0, corresponding to the different AR : H_2O_2 ratios are shown in relation to the reaction nanochannel in which they were obtained.

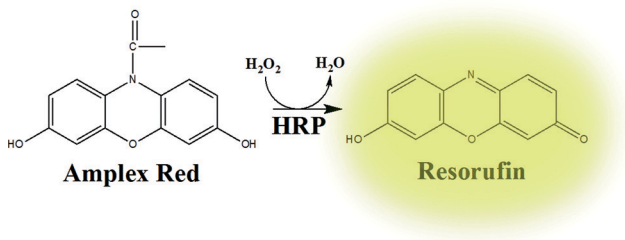

Scheme 1

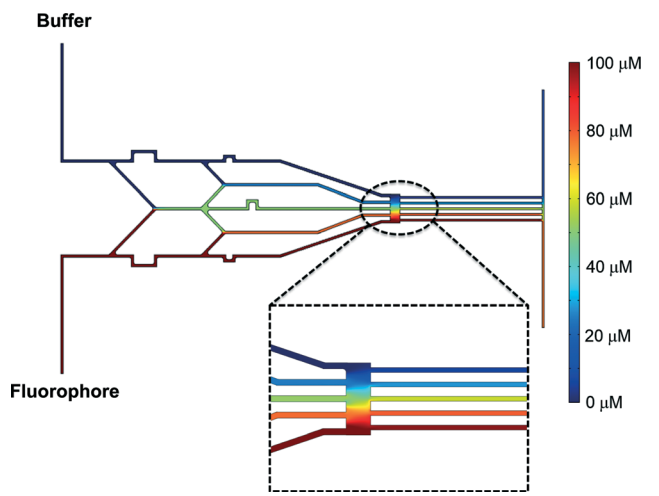

Fig. 2 Finite element simulations demonstrate concentration distribution within the gradient mixer. The enlarged view shows the species concentration for the each of the nanofluidic reaction channels.

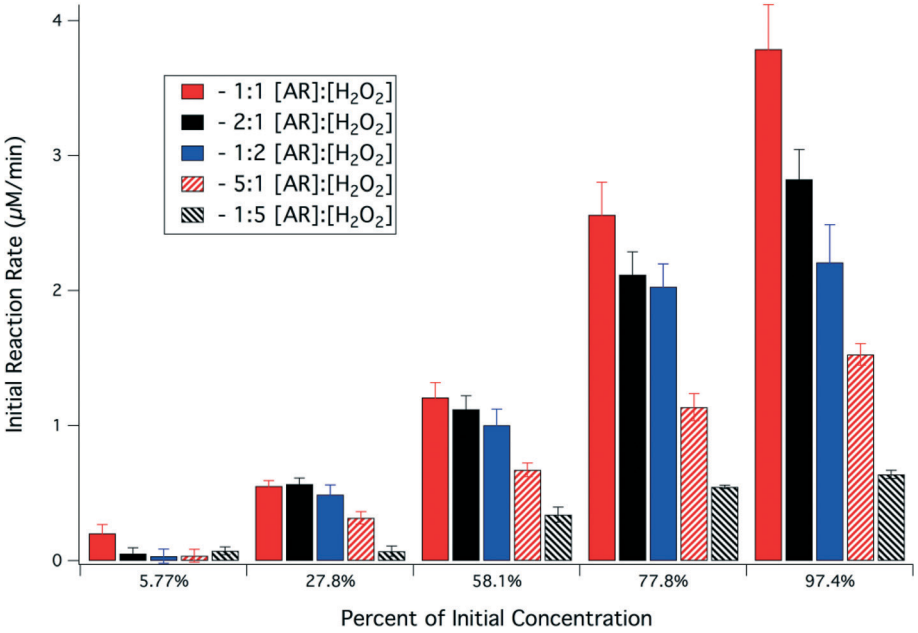

Fig. 3 Initial reaction rate as a function of initial reactant concentration ratio measured in the gradient mixer nanochannels. Initial reaction rate represents the initial slope of product formation with respect to time in Fig. S3.† Percent concentration represents the dilution factor from the initial 100 μM concentration of AR and H_2O_2. AR : H_2O_2 ratios of 1 : 1, 2 : 1, 1 : 2, 5 : 1, and 1 : 5 were examined. Error bars are ±1 standard deviation of the initial rate.

Starting AR : H_2O_2 reactant ratios of 1 : 1, 1 : 2, 1 : 5, 2 : 1, and 5 : 1 AR : H_2O_2 were chosen to determine the effect of concentration ratio on reaction kinetics. Under all concentrations 1 : 1 AR : H_2O_2 yielded the highest initial reaction velocity in each of the reaction channels, and the reaction velocity increases, as expected, with concentration from ~6 μM to ~97 μM for all reactant ratios. At the lowest overall concentration (highest dilution), 1 : 1 AR : H_2O_2 exhibits the largest r_0, while the other ratios yield statistically indistinguishable rates. Under these conditions we estimate a second order rate constant, $k = 6.8 \pm 0.7\ M^{-1}\ s^{-1}$. For the remainder of the conditions r_0 decreases in the order, 2 : 1, 1 : 2, 5 : 1, and 1 : 5, *i.e.* the larger the concentration mismatch the slower the initial velocity. In addition, in comparing 1 : *n* to *n* : 1 (*n* = 2, 5) AR : H_2O_2 ratios, the condition with excess H_2O_2 yields slower velocities across all conditions. This is consistent with the fact that under all conditions there is sufficient H_2O_2 to carry out the initial HRP oxidation to the Fe(IV) oxo species. After this, the active site catalyzes a one-electron transfer from Amplex Red yielding a radical intermediate.[17] Within this context, decreasing the amount of AR available for the second step would result in a slower reaction velocity.

Previous work from our laboratory[27] demonstrated that HRP-catalyzed conversion of AR to resorufin using immobilized HRP in a vertically-oriented (*i.e.* perpendicular to the substrate plane) nanopore yields higher initial rates, r_0, than free solution or planar bulk surface measurements. These experiments also compared non-stoichiometric AR : H_2O_2 ratios and yielded initial reaction rates ~1.6 times higher when AR is in excess compared to excess H_2O_2, similar to results obtained here with the nanofluidic mixer, *i.e.* a ratio of ~1.3 for 2 : 1 AR : H_2O_2 compared to 1 : 2 AR : H_2O_2 and an even greater difference, ~2.4, for 5 : 1 AR : H_2O_2 compared to 1 : 5 AR : H_2O_2.

Crowding measurements

Altering solution viscosity has been shown to affect macromolecular reaction kinetics. Increasing the solution viscosity is the most straightforward way to increase molecular crowding, and it has been shown to monotonically decrease the rates of diffusion-limited reactions and to increase them for reaction-limited situations.[43,46,47] Sucrose solutions with compositions 0, 5, 10, and 15 weight% sucrose in buffer (yielding viscosities of 1.0, 1.14, 1.33, and 1.59 cP, respectively) were used to increase the viscosity and therefore test its effect on r_0 in the HRP-catalyzed conversion of AR to resorufin. The voltage scheme and reactant introduction/dilution/mixing schemes used for these experiments were as depicted in Fig. 1. Fluorescence data were collected at a rate of 1 min^{-1} for 1 h, and the fluorescence data were again converted to resorufin concentration using the calibration in Fig. S2† and fit to give initial reaction velocities to compare against viscosity.

Fig. 4 shows the initial nanochannel reaction rates plotted against reactant concentration, expressed as a percentage of the initial 100 μM concentration, using 1 : 1 AR : H_2O_2 ratios for all viscosities. As expected, at all viscosities increasing the concentration of 1 : 1 AR : H_2O_2 increases r_0. Importantly, increasing solution viscosity lowers the initial reaction velocities, ranging from 0.01 μM min^{-1} to 0.19 μM min^{-1} at the highest value, η = 1.59 cP, to 0.21 μM min^{-1} l^{-1} to 3.79 μM min^{-1} for η = 1.00 cP. These observations are consistent with

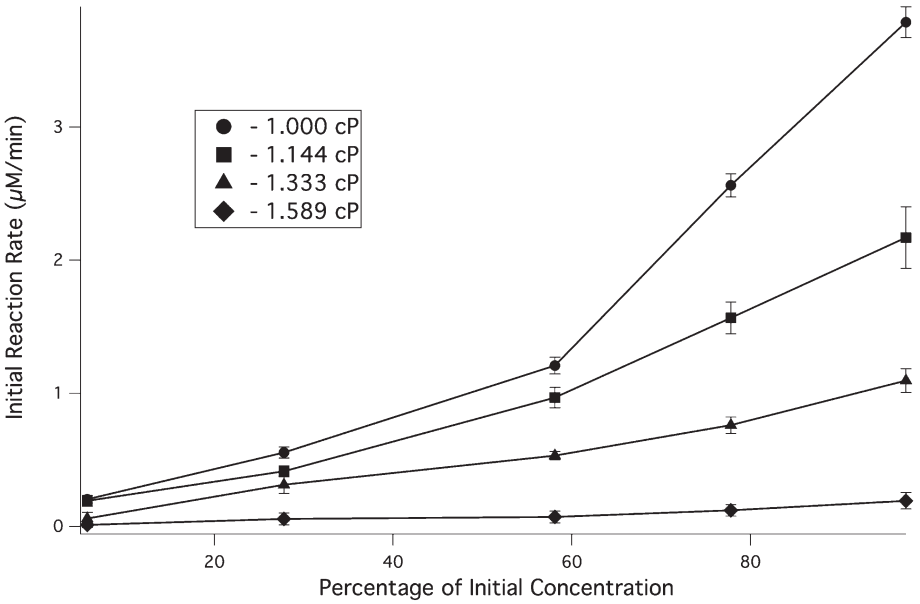

Fig. 4 Viscosity measurements. Initial reaction velocity as a function of initial reactant concentration measured in the reaction nanochannels. Initial reaction rate represents the slope of the product formation per unit time. Sucrose compositions range from 0–15% and had calculated viscosities from 1.0–1.6 cP. Error bars are ±1 standard deviation.

the HRP-catalyzed reaction being diffusion controlled under the conditions explored here, however the ~20-fold difference in r_0 between η = 1.00 cP and η = 1.59 cP greatly exceeds simple expectations based on differences in diffusion alone, as predicted, for example, by the Stokes–Einstein equation ($D \sim 1/\eta$). This suggests that in addition to its simple effect on reactant transport, crowding causes a change in the detailed dynamics governing the mechanism of HRP-catalyzed AR oxidation.

Conclusions

We have demonstrated a simple way to conduct multiple, simultaneous enzyme kinetics experiments using a nanofluidic gradient mixer. Starting with just two reactant concentrations, intersecting channels meet and mix the reactants to form a concentration gradient in the gradient column of the device. This concentration gradient is used to introduce different concentrations of analyte into a series of laterally displaced reaction nanochannels. The design of the mixer with a lateral diffusion zone at the end of the gradient mixing portion of the device allows for efficient an smooth concentration variations across the device that are consistent with the results of finite-element modeling calculations. This design may be altered to increase the degree of mixing by changing the structure of the mixing region or the number of reaction conditions, by simply increasing the number of reaction nanochannels.

Altering the AR : H_2O_2 ratio was observed to have a dramatic effect on the initial reaction velocities in this nanofluidic geometry, with concentration mismatches showing a decrease in initial velocity in all cases, with a stronger decrease when H_2O_2 is in excess. These observations are consistent with recent developments in understanding the mechanism of HRP-catalyzed oxidation of AR to resorufin. Increasing the viscosity inside the nanochannels results in a decrease in reaction velocity, consistent with diffusion-control, but the magnitude of the decrease suggests a crowding-induced effect on the mechanism of enzyme catalysis.

Acknowledgements

This work was supported by the Department of Energy under grant DE FG02 07ER15851 (WRAW) and a subcontract from Oak Ridge National Laboratory (DE-AC05-00OR22725; Subaward # 4000132808 – DH). The authors gratefully acknowledge the assistance of S. Branagan in the initial design of the gradient mixer. Fabrication of the devices studied here was accomplished at the Notre Dame Nanofabrication Facility whose generous support is gratefully acknowledged.

References

1 L. Yi, X. Wang, R. Dhumpa, A. M. Schrell, N. Mukhitov and M. G. Roper, *Lab Chip*, 2015, **15**, 823–832.
2 A. S. Johnson, K. B. Anderson, S. T. Halpin, D. C. Kirkpatrick, D. M. Spence and R. S. Martin, *Analyst*, 2013, **138**, 129–136.
3 D. C. Duffy, J. C. McDonald, O. J. A. Schueller and G. M. Whitesides, *Anal. Chem.*, 1998, **70**, 4974–4984.
4 K. B. Anderson, S. Y. Lockwood, R. S. Martin and D. M. Spence, *Anal. Chem.*, 2013, **85**, 5622–5626.
5 K. B. Anderson, S. T. Halpin, A. S. Johnson, R. S. Martin and D. M. Spence, *Analyst*, 2013, **138**, 137–143.
6 R. S. Martin, P. D. Root and D. M. Spence, *Analyst*, 2006, **131**, 1197–1206.

7 M. G. Roper and C. Guillo, *Anal. Bioanal. Chem.*, 2009, **393**, 459–465.
8 A. G. Hadd, D. E. Raymond, J. W. Halliwell, S. C. Jacobson and J. M. Ramsey, *Anal. Chem.*, 1997, **69**, 3407–3412.
9 G. H. Seong, J. Heo and R. M. Crooks, *Anal. Chem.*, 2003, **75**, 3161–3167.
10 D. C. Duffy, H. L. Gillis, J. Lin, N. F. Sheppard and G. J. Kellogg, *Anal. Chem.*, 1999, **71**, 4669–4678.
11 T. C. Kuo, D. M. Cannon, M. A. Shannon, P. W. Bohn and J. V. Sweedler, *Sens. Actuators, A*, 2003, **102**, 223–233.
12 A. Piruska, S. P. Branagan, A. B. Minnis, Z. Wang, D. M. Cropek, J. V. Sweedler and P. W. Bohn, *Lab Chip*, 2010, **10**, 1237–1244.
13 D. G. Haywood, A. Saha-Shah, L. A. Baker and S. C. Jacobson, *Anal. Chem.*, 2015, **87**, 172–187.
14 L. R. Gibson, S. P. Branagan and P. W. Bohn, *Small*, 2013, **9**, 90–97.
15 C. X. Ma, L. P. Zaino and P. W. Bohn, *Chem. Sci.*, 2015, **6**, 3173–3179.
16 Y. H. Lanyon, G. De Marzi, Y. E. Watson, A. J. Quinn, J. P. Gleeson, G. Redmond and D. W. M. Arrigan, *Anal. Chem.*, 2007, **79**, 3048–3055.
17 H. H. Gorris and D. R. Walt, *J. Am. Chem. Soc.*, 2009, **131**, 6277–6282.
18 L. D. Menard and J. M. Ramsey, *Nano Lett.*, 2011, **11**, 512–517.
19 C. A. Baker and M. G. Roper, *J. Chromatogr. A*, 2010, **1217**, 4743–4748.
20 D. G. Haywood, Z. D. Harms and S. C. Jacobson, *Anal. Chem.*, 2014, **86**, 11174–11180.
21 C. X. Ma, N. M. Contento, L. R. Gibson and P. W. Bohn, *ACS Nano*, 2013, **7**, 5483–5490.
22 J. M. Perry, K. M. Zhou, Z. D. Harms and S. C. Jacobson, *ACS Nano*, 2010, **4**, 3897–3902.
23 P. Mao and J. Y. Han, *Lab Chip*, 2005, **5**, 837–844.
24 Z. D. Harms, D. G. Haywood, A. R. Kneller, L. Selzer, A. Zlotnick and S. C. Jacobson, *Anal. Chem.*, 2015, **87**, 699–705.
25 S. P. Branagan, N. M. Contento and P. W. Bohn, *J. Am. Chem. Soc.*, 2012, **134**, 8617–8624.
26 J. de Jong, R. G. H. Lammertink and M. Wessling, *Lab Chip*, 2006, **6**, 1125–1139.
27 Z. Wang, T. L. King, S. P. Branagan and P. W. Bohn, *Analyst*, 2009, **134**, 851–859.
28 L. R. Gibson and P. W. Bohn, *Interface Focus*, 2013, **3**, 20120096.
29 M. L. Bruening, D. M. Dotzauer, P. Jain, L. Ouyang and G. L. Baker, *Langmuir*, 2008, **24**, 7663–7673.
30 P. Jain, G. L. Baker and M. L. Bruening, in *Annual Review of Analytical Chemistry*, Annual Reviews, Palo Alto, 2009, vol. 2, pp. 387–408.
31 F. Xu, W. H. Wang, Y. J. Tan and M. L. Bruening, *Anal. Chem.*, 2010, **82**, 10045–10051.
32 S. J. Li, C. Wang, Z. Q. Wu, J. J. Xu, X. H. Xia and H. Y. Chen, *Chem. – Eur. J.*, 2010, **16**, 10186–10194.
33 C. Wang, D. K. Ye, Y. Y. Wang, T. Lu and X. H. Xia, *Lab Chip*, 2013, **13**, 1546–1553.
34 J. Zhao, S. P. Branagan and P. W. Bohn, *Appl. Spectrosc.*, 2012, **66**, 163–169.
35 J. C. Yu, Y. J. Zhang and S. Q. Liu, *Biosens. Bioelectron.*, 2014, **55**, 307–312.
36 G. I. Berglund, G. H. Carlsson, A. T. Smith, H. Szoke, A. Henriksen and J. Hajdu, *Nature*, 2002, **417**, 463–468.
37 C. Wang, S. J. Li, Z. Q. Wu, J. J. Xu, H. Y. Chen and X. H. Xia, *Lab Chip*, 2010, **10**, 639–646.
38 A. Boveris, E. Martino and A. O. M. Stoppani, *Anal. Biochem.*, 1977, **80**, 145–158.
39 M. J. Zhou, Z. J. Diwu, N. PanchukVoloshina and R. P. Haugland, *Anal. Biochem.*, 1997, **253**, 162–168.
40 W. C. Yeon, B. Kannan, T. Wohland and V. Ng, *Langmuir*, 2008, **24**, 12142–12149.
41 A. S. Verkman, *Trends Biochem. Sci.*, 2002, **27**, 27–33.
42 J. A. Dix and A. S. Verkman, *Annu. Rev. Biophys.*, 2008, **37**, 247–263.
43 H. X. Zhou, G. N. Rivas and A. P. Minton, *Annu. Rev. Biophys.*, 2008, **37**, 375–397.
44 D. Amarie, J. A. Glazier and S. C. Jacobson, *Anal. Chem.*, 2007, **79**, 9471–9477.
45 A. Piruska, M. Gong, J. V. Sweedler and P. W. Bohn, *Chem. Soc. Rev.*, 2009, **38**, 1–13.
46 Y. Li, Y. Z. Xu, X. J. Feng and B. F. Liu, *Anal. Chem.*, 2012, **84**, 9025–9032.
47 C. Liu, Y. Li, Y. Li, P. Chen, X. Feng, W. Du and B.-F. Liu, *Talanta*, 2016, **149**, 237–243.